A revisit to the Cercignani–Lampis model: Langevin picture and its numerical simulation

AUTHOR(S):

Takata, Shigeru; Akasobe, Shigenori; Hattori, Masanari

A revisit to the Cercignani–Lampis model: Langevin picture and its numerical simulation

Shigeru Takata, Shigenori Akasobe, and Masanari Hattori

Abstract The Cercignani–Lampis (CL) model for the gas–surface interaction is revisited from the Langevin dynamics viewpoint. Starting from a time-independent Fokker–Planck formalism by Cercignani, its time-dependent extension and the corresponding Langevin description are introduced. The Langevin description sheds light on dynamical features of a stochastic process corresponding to the CL model. Numerical simulations on the basis of the Langevin description are performed as well to reproduce the scattering kernel and reflection intensity distribution numerically. Although the noise in the stochastic process is apparently simple, the Milstein scheme rather than the Euler–Maruyama scheme has to be adopted to achieve a satisfactory numerical convergence in time discretisation.

1 Introduction

Gas flows in low pressure and small-scale circumstances, which we generically call rarefied gas flows, require the kinetic theory description rather than the usual fluid dynamics description because the latter is implicitly limited to the local equilibrium states [16, 4]. Inter-molecular collisions inside the gas are not necessarily frequent in such circumstances, and sometimes molecular velocities inside the gas can be traced back without changes to the velocities just after the reflection on a container surface, a wall. Hence, the velocity distribution of reflected molecules can have a

S. Takata and M. Hattori
Department of Aeronautics and Astronautics, Kyoto University, Kyoto 615-8540, Japan , e-mail: takata.shigeru.4a@kyoto-u.ac.jp (S. Takata)
Research Project of Fluid Science and Engineering, Advanced Engineering Research Center, Kyoto University, Kyoto 615-8540, Japan

S. Akasobe
Department of Aeronautics and Astronautics, Kyoto University, Kyoto 615-8540, Japan.

direct impact on the gas behavior in the bulk region. An enough simple but realistic gas–surface interaction model has been desired for a long time.

Many efforts have been devoted even in rather recent years by Molecular Dynamics (MD), theoretical, and experimental approaches (e.g., [18, 1, 2] and references therein; a very good survey of the gas–surface interaction models before 90's can be found in [4]). Nevertheless, the progress so far is not necessarily satisfactory, probably due to difficulties of background physics in such interface problems. Even now, the diffuse reflection condition and/or its convex combination with the specular reflection condition, the so-called Maxwell condition, are primarily used and regarded as the standard in the literature [16, 4]. The former implicitly assumes perfect accommodation of incident molecules with the wall and reproduces the Lambert cosine law of the reflection intensity, while the latter is introduced by Maxwell to take account of imperfect accommodation. Although the latter reproduces some effects of the imperfect accommodation at a macroscopic level, the specular reflection part induces a spike in the reflection intensity distribution, which is different from observations in molecular beam experiments.

After Maxwell, the concept of accommodation has been developed to introduce different coefficients to represent a possible difference of accommodation in momentum and energy exchanges [15, 11, 4]. Cercignani and Lampis [5] proposed in 1971 a mathematical physical model, which is now called the Cercignani–Lampis (CL) model. A similar model was independently proposed by Kŭscer et al. [12]. Their models have an impact in their capability to reproduce typical features of the reflection intensity distributions experimentally observed.

The CL model has been enjoying successful practical applications, including its extension and easy implementation [13] to the Direct Simulation Monte Carlo (DSMC) algorithm since 90's. Nevertheless, it seems that the dynamical background is still behind a mysterious veil, though its physical interpretation and alternative derivation were reported in 70's (e.g., [17, 6]). No further attempts have been made to shed light on the dynamical aspects of the model. It is the main motivation of the present study.

In the present paper, we discuss the CL model mainly along the lines laid by Cercignani in [4]. We, however, modify his original discussions for a time-dependent problem in order to have a stochastic dynamical picture, the Langevin equation description. Results of numerical simulations and scheme accuracy in time discretisation will be presented as well.

2 Scattering kernel and Cercignani–Lampis (CL) model

Let us denote by $f(t,\boldsymbol{x},\boldsymbol{\xi})$ the velocity distribution function of gas molecules, where t is a time, $\boldsymbol{x}$ is a position, and $\boldsymbol{\xi}$ is a molecular velocity. Assuming that a resting solid wall occupies the region $x_1 < 0$, the reflection law for gas molecules on the wall is expressed as

$$f(t,\boldsymbol{x}_\parallel,x_1=0,\boldsymbol{\xi})=\int_{\overline{\xi}_1<0}K(\boldsymbol{x}_\parallel,\boldsymbol{\xi},\overline{\boldsymbol{\xi}})f(t,\boldsymbol{x}_\parallel,x_1=0,\overline{\boldsymbol{\xi}})d\overline{\boldsymbol{\xi}},\quad \xi_1>0, \tag{1}$$

or equivalently as

$$\xi_1 f(t,\boldsymbol{x}_\parallel,x_1=0,\boldsymbol{\xi})=\int_{\overline{\xi}_1<0}\mathcal{R}(\boldsymbol{x}_\parallel,\boldsymbol{\xi},\overline{\boldsymbol{\xi}})|\overline{\xi}_1|f(t,\boldsymbol{x}_\parallel,x_1=0,\overline{\boldsymbol{\xi}})d\overline{\boldsymbol{\xi}},\quad \xi_1>0. \tag{2}$$

Here $\boldsymbol{x}_\parallel=(x_2,x_3)$, which will be suppressed mostly in what follows because the discussion is not concerned with the variation of K (or $\mathcal{R}$) in that direction. In the present paper, we shall call K the scattering kernel and $\mathcal{R}$ the reflection probability, respectively. [1] They are related to each other as

$$|\xi_1|K(\boldsymbol{\xi},\overline{\boldsymbol{\xi}})=|\overline{\xi}_1|\mathcal{R}(\boldsymbol{\xi},\overline{\boldsymbol{\xi}}), \tag{3}$$

and are usually supposed to be independent of f both in physics and mathematics. Physically, it implies that the microscopic properties of the wall do not change by the interaction with the gas. We follow this convention, and thus the right-hand sides of (1) and (2) are linear with respect to f. Experiments of mono-collimated molecular beam scattering are performed on the basis of the same convention, though it is not explicitly mentioned. In the case of the diffuse reflection condition, the scattering kernel reads

$$K=\frac{|\overline{\xi}_1|}{2\pi(RT_w)^2}\exp(-\frac{|\boldsymbol{\xi}|^2}{2RT_w}), \tag{4}$$

where T_w is the wall temperature and R is the specific gas constant (the Boltzmann's constant k_B divided by the mass of a molecule m; $R=k_B/m$). Cercignani and Lampis [5] proposed the following form of the scattering kernel:

$$K=\frac{|\overline{\xi}_1|}{2\pi(RT_w)^2}\frac{1}{\alpha_t(2-\alpha_t)\alpha_n}I_0(\frac{\xi_1\overline{\xi}_1}{RT_w}\frac{\sqrt{1-\alpha_n}}{\alpha_n})\exp(-\frac{\xi_1^2+\overline{\xi}_1^2(1-\alpha_n)}{2RT_w\alpha_n})$$
$$\times\exp(-\frac{|\boldsymbol{\xi}_\parallel-\overline{\boldsymbol{\xi}}_\parallel(1-\alpha_t)|^2}{2RT_w\alpha_t(2-\alpha_t)}), \tag{5}$$

where $\boldsymbol{\xi}_\parallel=(\xi_2,\xi_3)$ and I_0 is the modified Bessel function of the first kind and zeroth order:

$$I_0(x)\equiv\frac{1}{2\pi}\int_0^{2\pi}\exp(x\cos\varphi)d\varphi. \tag{6}$$

The boundary condition (1) with the kernel (5) is called the Cercignani–Lampis (CL) model and contains two adjustable parameters: $0\le\alpha_n\le1$ and $0\le\alpha_t\le2$. When $\alpha_n=\alpha_t=1$, it recovers the diffuse reflection condition (4).

[1] We have adopted the terminology in [16]. In [4], $\mathcal{R}$ is called the scattering kernel, which is a flux based terminology like (2). As $\int_{\xi_1>0}\mathcal{R}d\boldsymbol{\xi}=1$ and $\mathcal{R}\ge0$, $\mathcal{R}$ can be interpreted as the probability density of finding a reflected molecule at a specific value of the velocity.

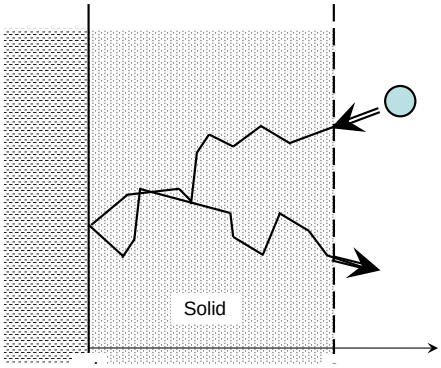

Fig. 1 Schematics of scattering of a gas molecule

3 Cercignani's Fokker–Planck (FP) system

In [3], Cercignani introduced a time-independent Fokker–Planck system for the probability density $P(x_1, \boldsymbol{\xi})$ of a molecule at position x_1 with velocity $\boldsymbol{\xi}$. It reproduces the CL model in the parameter range $0 \le \alpha_n \le 1$ and $0 \le \alpha_t \le 1$ and reads

$$\xi_1 \frac{\partial P}{\partial x_1} + \frac{\partial P}{\partial \xi_i} X_i = LP, \quad (-d < x_1 < 0), \tag{7a}$$

$$LP = \frac{\partial^2}{\partial \xi_j \partial \xi_i} \left(D_{ij} P \right) + \frac{\partial}{\partial \xi_i} \left[\left(F_{ij} \xi_j - \frac{\partial D_{ij}}{\partial \xi_j} \right) P \right], \tag{7b}$$

$$\text{b.c. } P(x_1 = 0, \xi_1 < 0, \boldsymbol{\xi}_\parallel) = \delta(\boldsymbol{\xi} - \boldsymbol{\xi}_{\text{in}}), \tag{7c}$$

$$P(x_1 = -d, \xi_1, \boldsymbol{\xi}_\parallel) = P(x_1 = -d, -\xi_1, \boldsymbol{\xi}_\parallel), \quad \xi_1 > 0. \tag{7d}$$

Here $\boldsymbol{\xi}_{\text{in}}$ is the molecular velocity of incidence, the interaction with the wall is supposed to occur in $x_1 < 0$, and $x_1 = -d$ is the position of the potential barrier beyond which a molecule is forbidden to proceed (Fig. 1). The X_i, D_{ij}, and F_{ij} in the above are defined as follows:

$$X_i = 0, \quad D_{11} = \frac{2RT_w}{\ell_n} |\xi_1|, \quad D_{22} = D_{33} = \frac{2RT_w}{\ell_t} |\xi_1|, \tag{7e}$$

$$D_{ij} = 0 \quad (i \ne j), \quad F_{ij} = \frac{1}{RT_w} D_{ij}, \tag{7f}$$

where ℓ_t and ℓ_n are a characteristic length of molecular velocity diffusion in the x_2x_3-plane and that in the x_1-direction, respectively. By solving the above system (7), we have the velocity distribution $P(x_1 = 0, \xi_1 > 0, \boldsymbol{\xi}_\parallel)$ of reflected molecules against the incident molecular beam $\delta(\boldsymbol{\xi} - \boldsymbol{\xi}_{\text{in}})$. Substitution of $f = \delta(\boldsymbol{\xi} - \boldsymbol{\xi}_{\text{in}})$ into (1) or (2) gives the relation

$$\mathcal{R}(\xi_1 > 0, \boldsymbol{\xi}_{\rm in}) = \frac{|\xi_1|}{|\xi_{\rm in1}|} K(\xi_1 > 0, \boldsymbol{\xi}_{\rm in}) = \frac{|\xi_1|}{|\xi_{\rm in1}|} P(x_1 = 0, \xi_1 > 0), \tag{8}$$

(see [4, Sec. III. 2, Eq. (2.12)]). Hence, finding the form of K is identical to finding P at $x_1 = 0$ for $\xi_1 > 0$. Here and in what follows, we suppress $\boldsymbol{\xi}_{\parallel}$ in the argument of K etc., if no confusion is expected.

4 From Fokker–Planck to Langevin system

The time-independent Fokker–Planck (FP) system in Sec. 3 is the starting point of our discussions. We first introduce its simple but natural extension to the time-dependent situation. Then, we identify the Langevin system, namely the stochastic dynamics of a test particle, which is equivalent to the extended system.

4.1 Time-dependent Fokker–Planck system

In order to draw out a dynamical picture behind the CL model, we simply add a time derivative term to the left-hand side of (7a), allow the spatial dependence in (x_2, x_3)-directions, and modify the condition (7c) in accordance with the time and spatial localization of the incident molecular beam. Then, we have the following initial- and boundary-value problem:

$$\frac{\partial Q}{\partial t} = -\xi_i \frac{\partial Q}{\partial x_i} + \frac{\partial^2}{\partial \xi_j \partial \xi_i} \left(D_{ij} Q \right) + \frac{\partial}{\partial \xi_i} \left[\left(F_{ij} \xi_j - \frac{\partial D_{ij}}{\partial \xi_j} \right) Q \right], \ (-d < x_1 < 0), \tag{9a}$$

$$\text{b.c. } Q(t, \boldsymbol{x}, \boldsymbol{\xi}) = \delta(t) \delta(\boldsymbol{x}) \delta(\boldsymbol{\xi} - \boldsymbol{\xi}_{\rm in}), \quad \xi_1 < 0, \quad x_1 = 0, \tag{9b}$$

$$Q(t, x_1 = -d, \xi_1) = Q(t, x_1 = -d, -\xi_1), \quad \xi_1 > 0, \tag{9c}$$

where $Q(t, \boldsymbol{x}, \boldsymbol{\xi})$ is the probability density finding a molecule at time t, position $\boldsymbol{x}$, and velocity $\boldsymbol{\xi}$. As Q is the fundamental solution (the Green function) to the initial- and boundary-value problems for the same FP equation, we switch its notation to $G(0, \boldsymbol{0}, \boldsymbol{\xi}_{\rm in}; t, \boldsymbol{x}, \boldsymbol{\xi})$ from now on. Here, the first three arguments of G indicate that the time, position, and velocity of incidence are $t = 0$, $\boldsymbol{x} = 0$, and $\boldsymbol{\xi} = \boldsymbol{\xi}_{\rm in}$, respectively. Since the microscopic property of the wall, or the coefficients D_{ij} and F_{ij}, are independent of t and $\boldsymbol{x}_{\parallel}$, the solution is invariant under the translation both in time and in the $x_2 x_3$-plane:

$$G(s, \boldsymbol{x}_{\rm in}, \boldsymbol{\xi}_{\rm in}; t, \boldsymbol{x}, \boldsymbol{\xi}) = G(0, \boldsymbol{0}, \boldsymbol{\xi}_{\rm in}; t - s, \boldsymbol{x} - \boldsymbol{x}_{\rm in}, \boldsymbol{\xi}), \quad s \le t, \tag{10}$$

where $\boldsymbol{x}_{\rm in} = (0, \boldsymbol{x}_{\rm in\parallel})$. This motivates us to define $\overline{G} \equiv \int_{-\infty}^{t} \int_{\mathbb{R}^2} G(s, \boldsymbol{x}_{\rm in}, \boldsymbol{\xi}_{\rm in}; t, \boldsymbol{x}, \boldsymbol{\xi}) d\boldsymbol{x}_{\parallel} ds$. The following property holds:

$$\begin{aligned}\overline{G} &= \int_{-\infty}^{t}\int_{\mathbb{R}^2} G(s,\boldsymbol{x}_{\rm in},\boldsymbol{\xi}_{\rm in};t,\boldsymbol{x},\boldsymbol{\xi})d\boldsymbol{x}_{\parallel}ds \\ &= \int_{-\infty}^{t}\int_{\mathbb{R}^2} G(0,\boldsymbol{0},\boldsymbol{\xi}_{\rm in};t-s,\boldsymbol{x}-\boldsymbol{x}_{\rm in},\boldsymbol{\xi})d\boldsymbol{x}_{\parallel}ds \\ &= \int_{0}^{\infty}\int_{\mathbb{R}^2} G(0,\boldsymbol{0},\boldsymbol{\xi}_{\rm in};\tau,\boldsymbol{x},\boldsymbol{\xi})d\boldsymbol{x}_{\parallel}d\tau. \end{aligned} \tag{11}$$

It is seen from the last equality that $\overline{G}$ is a solution of (9a) independent of $\boldsymbol{x}_{{\rm in}\parallel}$ as well as t and $\boldsymbol{x}_{\parallel}$; accordingly it will be denoted as $\overline{G}(\boldsymbol{\xi}_{\rm in};x_1,\boldsymbol{\xi})$. Note that $\overline{G}$ solves (7a) as well. It is readily seen from (9b) and (9c) that $\overline{G}$ satisfies the conditions (7c) and (7d). Thus, $\overline{G}$ is a solution of the system (7).

In Sec. 4.2, we present the Langevin system corresponding to the above system (9). The observation on $\overline{G}$ tells that the scattering kernel K is identical with $\overline{G}(\boldsymbol{\xi}_{\rm in};x_1=0,\boldsymbol{\xi})$ and thus can be constructed from G. This implies that the kernel of the CL model can be reproduced by many samples of a test particle simulation of the Langevin system. We will come back to this issue in Sec. 5.2.

4.2 Langevin system for the CL model: A stochastic dynamical picture

We first consider the following Langevin equation:

$$dx_i = \xi_i dt, \quad d\xi_i = (-\gamma_{ij}\xi_j + F_i)dt + S_{ij}dW_j, \tag{12}$$

where W_j is the Wiener process that satisfies $\langle dW_i dW_j\rangle = dt\,\delta_{ij}$. Just for convenience, let us introduce a six-dimensional vector variable y_α ($\alpha=1,\ldots,6$) defined by $y_i = x_i$ and $y_{i+3}=\xi_i$ ($i=1,\ldots,3$) and rewrite (12) as follows:

$$dy_\alpha = (A_{\alpha\beta}y_\beta + B_\alpha)dt + \Theta_{\alpha i}dW_i, \tag{13a}$$

where

$$[A_{\alpha\beta}] = \begin{bmatrix} 0&0&0&1&0&0\\ 0&0&0&0&1&0\\ 0&0&0&0&0&1\\ 0&0&0&-\gamma_{11}&-\gamma_{12}&-\gamma_{13}\\ 0&0&0&-\gamma_{21}&-\gamma_{22}&-\gamma_{23}\\ 0&0&0&-\gamma_{31}&-\gamma_{32}&-\gamma_{33} \end{bmatrix}, \tag{13b}$$

$$[B_\alpha] = \begin{bmatrix} 0 \\ 0 \\ 0 \\ F_1 \\ F_2 \\ F_3 \end{bmatrix}, \quad [\Theta_{\alpha i}] = \begin{bmatrix} 0 & 0 & 0 \\ 0 & 0 & 0 \\ 0 & 0 & 0 \\ S_{11} & S_{12} & S_{13} \\ S_{21} & S_{22} & S_{23} \\ S_{31} & S_{32} & S_{33} \end{bmatrix}. \tag{13c}$$

The corresponding Fokker–Planck equation is known to take the following form [7]:

$$\frac{\partial g}{\partial t} = -\frac{\partial}{\partial y_\alpha}([A_{\alpha\beta} y_\beta + B_\alpha] g) + \frac{1}{2}\frac{\partial^2}{\partial y_\alpha \partial y_\beta}(\Theta_{\alpha i}\Theta_{\beta i} g). \tag{14}$$

Using the original pair of three-dimensional vector variables (x_i, ξ_i) in place of y_α, (14) is rewritten as

$$\frac{\partial g}{\partial t} = -\frac{\partial}{\partial x_i}(\xi_i g) - \frac{\partial}{\partial \xi_i}(-\gamma_{ij}\xi_j g + F_i g) + \frac{1}{2}\frac{\partial^2}{\partial \xi_i \partial \xi_j}(S_{ik} S_{jk} g). \tag{15}$$

Now, comparing (15) and (9a) leads us to find the correspondence of coefficients:

$$\frac{1}{2} S_{ik} S_{jk} = D_{ij}, \quad \gamma_{ij}\xi_j - F_i = F_{ij}\xi_j - \frac{\partial D_{ij}}{\partial \xi_j}. \tag{16}$$

Note that, because of the definition (7e),

$$\frac{\partial D_{ij}}{\partial \xi_j} = \frac{\xi_1}{|\xi_1|}\frac{2RT_w}{\ell_n}\delta_{i1}. \tag{17}$$

Thus, γ_{ij}, S_{ij}, and F_i are identified as

$$\gamma_{ij} = F_{ij} = \frac{1}{RT_w} D_{ij} = 2\left[\frac{|\xi_1|}{\ell_n}\delta_{i1}\delta_{j1} + \frac{|\xi_1|}{\ell_t}(\delta_{i2}\delta_{j2} + \delta_{i3}\delta_{j3})\right], \tag{18a}$$

$$F_i = \frac{\xi_1}{|\xi_1|}\frac{2RT_w}{\ell_n}\delta_{i1}, \tag{18b}$$

$$S_{ij} = 2\sqrt{RT_w \frac{|\xi_1|}{\ell_n}}\delta_{i1}\delta_{j1} + 2\sqrt{RT_w \frac{|\xi_1|}{\ell_t}}(\delta_{i2}\delta_{j2} + \delta_{i3}\delta_{j3}). \tag{18c}$$

Here, we have chosen S_{ij} to be symmetric.

To summarize, we have identified the Langevin system corresponding to the time-dependent FP system (9):

$$dx_i = \xi_i dt, \quad (i = 1, 2, 3), \tag{19a}$$

$$d\xi_1 = -\frac{2}{\ell_n}\left(|\xi_1|\xi_1 - \frac{\xi_1}{|\xi_1|}RT_w\right)dt + 2\sqrt{RT_w \frac{|\xi_1|}{\ell_n}}\, dW_1, \tag{19b}$$

$$d\xi_2 = -\frac{2}{\ell_t}|\xi_1|\xi_2 dt + 2\sqrt{RT_w\frac{|\xi_1|}{\ell_t}}dW_2, \tag{19c}$$

$$d\xi_3 = -\frac{2}{\ell_t}|\xi_1|\xi_3 dt + 2\sqrt{RT_w\frac{|\xi_1|}{\ell_t}}dW_3, \tag{19d}$$

supplemented by the specular reflection at the potential barrier $x_1 = -d$ and the initial condition

$$\boldsymbol{x}(0) = \boldsymbol{0}, \quad \boldsymbol{\xi}(0) = \boldsymbol{\xi}_{\rm in}. \tag{19e}$$

5 Discussions

5.1 Dynamical aspects of the CL model

The Langevin system (19) tells that, after the incidence, the molecule changes its velocity under two types of interactions with the wall. One is the first term on the right-hand side of (19b)–(19d), which we call a *drift* part. The other is the second term on the same side of (19b)–(19d), while we call a *diffusion* part. Below we discard the spatial translation (19a) and concentrate on the dynamics described by (19b)–(19d). Before going into details, it should be noted that the motion in the normal direction is seen to be independent of those in tangential directions. The reverse is not true.

Role of the *drift* part

In the direction normal to the surface, the *drift* part decelerates a molecule if the kinetic energy $(1/2)m\xi_1^2$ in that direction is beyond the thermodynamic energy $(1/2)k_BT_w$ distributed by the equipartition law [8]. If not, it accelerates the molecule until the kinetic energy $(1/2)m\xi_1^2$ reaches that energy. To see the mechanism more closely, discard the second term in (19b) and integrate it in time. Then, we have for $\xi_1 < 0$

$$\xi_1 = -\sqrt{RT_w}\frac{1 \mp c_- \exp(-\frac{4\sqrt{RT_w}}{\ell_n}t)}{1 \pm c_- \exp(-\frac{4\sqrt{RT_w}}{\ell_n}t)}, \quad -\sqrt{RT_w} \leqq \xi_1 (< 0), \tag{20a}$$

and for $\xi_1 > 0$

$$\xi_1 = \sqrt{RT_w}\frac{1 \pm c_+ \exp(-\frac{4\sqrt{RT_w}}{\ell_n}t)}{1 \mp c_+ \exp(-\frac{4\sqrt{RT_w}}{\ell_n}t)}, \quad \sqrt{RT_w} \lesseqgtr \xi_1 (> 0), \tag{20b}$$

where $c_\pm$ is a positive constant not larger than unity. Hence, there is no reversal of motion in the normal direction if neither thermal noise nor potential barrier exist. The *drift* part thus drives ξ_1 towards $\pm\sqrt{RT_w}$ depending on its sign exponentially in time.[2]

In directions tangential to the surface, the *drift* part always decelerates the molecular motion in proportion to the momentum transferred by the incoming molecule, i.e., $-|\xi_1|\boldsymbol{\xi}_\parallel$, where $\boldsymbol{\xi}_\parallel = (\xi_2, \xi_3)$. Thus, it works on the molecule in a similar way to the viscous drag. To see the effect more closely, consider the motion in the x_2-direction. The motion in the x_3-direction follows the same dynamics, as is clear from (19c) and (19d). As before, discarding the second term in (19c) and integrating it in time give

$$\xi_2 = c_0 \exp(-\frac{2}{\ell_t}\int |\xi_1| dt), \tag{21}$$

where c_0 is a constant. Hence, as far as $\xi_1 \neq 0$, the *drift*-part force decelerates ξ_2 and makes it vanish if the integration of $|\xi_1|$ in time is not bounded. It is also seen that the larger $|\xi_1|$ is, the larger the decaying rate is.

Role of the *diffusion* part and competition with the *drift* part

In order to see the role of the *diffusion* part and its competition with the *drift* part, we go back to the time-dependent FP system, (9a) without the spatial translation term and (9b).

Let us first single out the *diffusion* part. The FP system without the spatial translation and the *drift* part admits a stationary solution inversely proportional to $|\xi_1|$ in the normal direction, provided that the integrability condition is discarded. In the tangential directions, it is just a usual diffusion process without center shifting, and only its time scale depends on $|\xi_1|$. A couple of examples of particle simulations of (19b) and (19c) without the *drift* part are shown in Figs. 2 (a) and (b), which clearly demonstrate those features. The *diffusion* part competes with the *drift* part to form the half-range Maxwellian in the normal direction and the full Maxwellian with the zero mean velocity in the tangential directions as a stationary state; see Figs. 2 (c) and (d). The admitted stationary solution under the competition corresponds to the full accommodation situation, namely the diffuse reflection model. In the CL model,

[2] Using the relation (31) that appears later, the exponential factor can be rewritten as

$$\exp(-\frac{4\sqrt{RT_w}}{\ell_n}t) = (1-\alpha_n)^{\frac{\sqrt{RT_w}}{2d}t}.$$

Hence, if $|\xi_1| < \sqrt{RT_w}$, the molecule stays longer than $2d/\sqrt{RT_w}$ in the interaction region, making the above factor smaller and smaller until leaving. If $|\xi_1| > \sqrt{RT_w}$, the molecule stays shorter, keeping the same factor between $1-\alpha_n$ and unity.

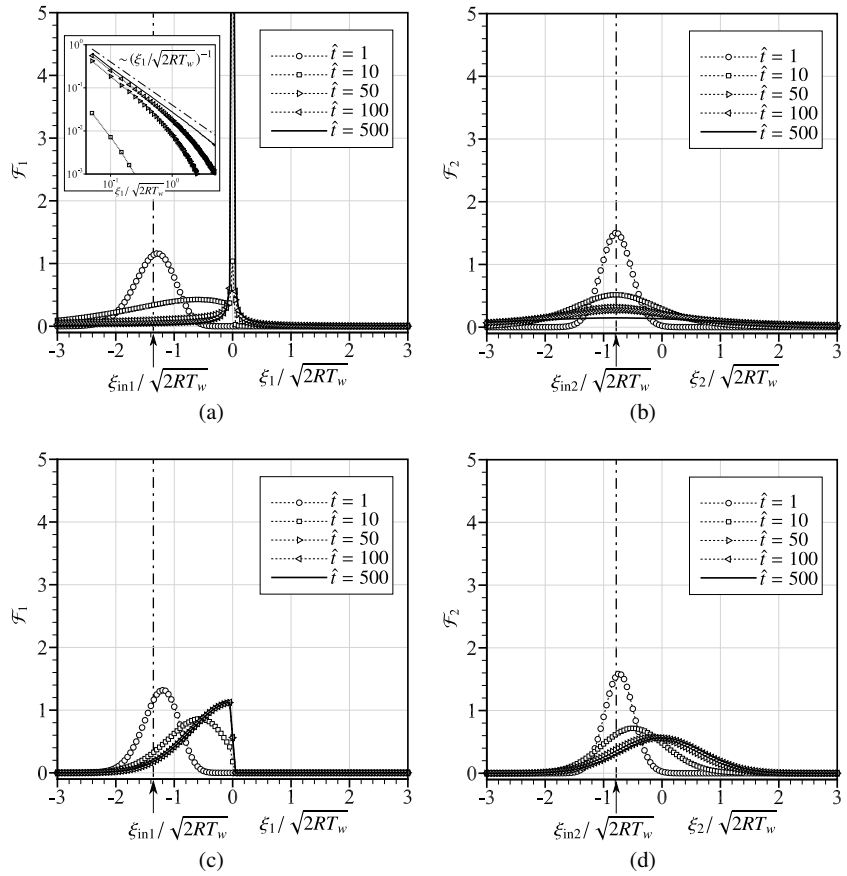

Fig. 2 The *diffusion*-part effect and the competition between the *drift* and the *diffusion* part in the case $|\boldsymbol{\xi}_{\rm in}|/\sqrt{2RT_w} = 1.56718$ with $(\xi_{\rm in2}, \xi_{\rm in3})/\sqrt{2RT_w} = (-0.78359, 0)$. No spatial translation is considered. (a) the *diffusion*-part effect in the normal direction, (b) the *diffusion*-part effect in the incident tangential direction, (c) the competition between the *drift*- and the *diffusion*-part in the normal direction, and (d) the competition between the *drift*- and the *diffusion*-part in the incident tangential direction. Here, $\hat{t} = (\sqrt{2RT_w}/\ell)t$ with ℓ being $\ell = -(1/8)(\ln 0.7)\ell_n = -(1/4)(\ln 0.9)\ell_t$ and $\mathcal{F}_\alpha(\xi_\alpha) = \sum_{i=1}^{N} \chi_{[\xi_\alpha, \xi_\alpha+\Delta\xi_\alpha]}(\xi_\alpha^{(i)})/(N\Delta\xi_\alpha/\sqrt{2RT_w})$ $(\alpha = 1, 2)$ with $\boldsymbol{\xi}^{(i)}$ and χ_A being the molecular velocity of the i-th sample of simulation and the characteristic function of A, respectively [see the sentence following (29) that appears later]. The Milstein scheme to be explained later is used with the timestep $\Delta t = 0.0002(\ell/\sqrt{2RT_w})$, and the number of sampling and the intervals for the histogram of $\mathcal{F}_\alpha$ in molecular velocity are respectively $N = 10^7$ and $\Delta\xi_1 = \Delta\xi_2 = 0.05\sqrt{2RT_w}$.

however, molecules spatially translate in the interaction region and may leave there before reaching the full accommodation.

5.2 Langevin system and the reflection intensity distribution

We first consider the way how to recover $\overline{G}$ from the samples (test particles) of the Langevin system simulation. The base of our discussion is the identity

$$\overline{G}(\overline{\boldsymbol{\xi}}; 0, \boldsymbol{\xi}) = \int_0^\infty \int_{\mathbb{R}^2} G(0, \mathbf{0}, \overline{\boldsymbol{\xi}}; \tau, x_1 = 0, \boldsymbol{x}_\parallel, \boldsymbol{\xi}) d\boldsymbol{x}_\parallel d\tau, \tag{22}$$

which has already appeared in Sec. 4.1. Remind that solving the Langevin system is identical to getting the above integrand G.

Taking account of the time and the spatial integration in (22), let us first count the number of sample molecular velocities at the instance of exit from the interaction region $x_1 < 0$, irrespective of the $\boldsymbol{x}_\parallel$ position and exit time. Then, $\mathcal{N}$ samples for the common velocity of incidence $\overline{\boldsymbol{\xi}}$ yields a normalized distribution in the molecular velocity:

$$\frac{1}{\mathcal{N}} \sum_{i=1}^{\mathcal{N}} \delta(\boldsymbol{\xi} - \boldsymbol{\xi}^{(i)}), \tag{23}$$

where $\boldsymbol{\xi}^{(i)}$ is the molecular velocity at the instance of exit in the i-th sample of simulation. The above simple counting is, however, not directly connected with $\overline{G}$ (or more precisely G) because $\overline{G}$ (or G) is the quantity that is concerned with the small interval $[0, dx_1]$. The time duration for which the molecule is in the small interval should have been taken into account in (23) to have a direct connection with $\overline{G}$. Hence, the counting with weight $dx_1/\xi_1^{(i)}$ should be taken

$$\overline{G}(\overline{\boldsymbol{\xi}}; 0, \boldsymbol{\xi}) dx_1 \propto \frac{1}{\mathcal{N}} \sum_{i=1}^{\mathcal{N}} \frac{dx_1}{\xi_1^{(i)}} \delta(\boldsymbol{\xi} - \boldsymbol{\xi}^{(i)}). \tag{24}$$

Remember that the left-hand side is nothing else than $K(\boldsymbol{\xi}, \overline{\boldsymbol{\xi}}) dx_1$. Thus, from (8) and $\int_{\xi_1 > 0} \mathcal{R}(\boldsymbol{\xi}, \overline{\boldsymbol{\xi}}) d\boldsymbol{\xi} = 1$ (see footnote 1), we arrive at the relation (in the sense of weak formulation) that

$$|\xi_1| \overline{G} = \frac{|\overline{\xi}_1|}{\mathcal{N}} \sum_{i=1}^{\mathcal{N}} \delta(\boldsymbol{\xi} - \boldsymbol{\xi}^{(i)}), \tag{25}$$

which establishes the way how to construct the scattering kernel from the Langevin system simulation.

Next, we proceed to the reflection intensity distribution. Introducing the polar coordinates (ξ, θ, φ) of the molecular velocity with positive x_1 being the polar direction, the normalized intensity distribution $I(\theta, \varphi)$ is expressed as

$$I(\theta,\varphi) = \frac{1}{I_{\rm in}} \int_0^\infty f(\boldsymbol{\xi})\, \xi \cos\theta\, \xi^2 d\xi, \quad \cos\theta > 0, \tag{26a}$$

$$I_{\rm in} = \int_{\overline{\xi}_1<0} |\overline{\xi}_1| f(\overline{\boldsymbol{\xi}}) d\overline{\boldsymbol{\xi}}, \tag{26b}$$

where f is the velocity distribution function of molecules on the wall. Substitution of (2) into (26a) gives

$$I(\theta,\varphi) = \frac{1}{I_{\rm in}} \int_0^\infty \left(\int_{\overline{\xi}_1<0} |\overline{\xi}_1| \mathcal{R}(\boldsymbol{\xi},\overline{\boldsymbol{\xi}}) f(\overline{\boldsymbol{\xi}}) d\overline{\boldsymbol{\xi}} \right) \xi^2 d\xi, \quad \xi_1 > 0. \tag{27}$$

In the case of the mono-collimated molecular beam, $f(\overline{\boldsymbol{\xi}}) = \delta(\overline{\boldsymbol{\xi}} - \boldsymbol{\xi}_{\rm in})$, the intensity distribution is reduced to

$$\begin{aligned} I(\theta,\varphi) = \int_0^\infty \mathcal{R}(\boldsymbol{\xi},\boldsymbol{\xi}_{\rm in})\, \xi^2 d\xi &= \frac{1}{|\xi_{\rm in1}|} \int_0^\infty \xi^2 \xi_1\, \overline{G}\, d\xi \\ &= \frac{1}{|\xi_{\rm in1}|} \int_0^\infty \xi^3 \cos\theta\, \overline{G}\, d\xi, \quad (\cos\theta > 0). \end{aligned} \tag{28}$$

Here it has been used that $I_{\rm in} = \int_{\overline{\xi}_1<0} |\overline{\xi}_1| \delta(\overline{\boldsymbol{\xi}} - \boldsymbol{\xi}_{\rm in}) d\overline{\boldsymbol{\xi}} = |\xi_{\rm in1}|$. Note that I follows the Lambert cosine law, if $\overline{G}$ is isotropic as the diffuse reflection case. The deviation from the cosine law implies the non-isotropy of $\overline{G}$. Now using (25), the intensity distribution can be reproduced by the following sample counting of the Langevin system simulation:

$$\begin{aligned} I\, \sin\theta \Delta\theta \Delta\varphi &= \frac{1}{\mathcal{N}} \sum_{i=1}^{\mathcal{N}} \int_0^\infty d\xi\, \xi^2 \int_\varphi^{\varphi+\Delta\varphi} d\varphi \int_\theta^{\theta+\Delta\theta} d\theta\, \sin\theta\, \frac{\delta(\xi - \xi^{(i)})\delta(\theta - \theta^{(i)})\delta(\varphi - \varphi^{(i)})}{\xi^2 \sin\theta} \\ &= \frac{1}{\mathcal{N}} \sum_{i=1}^{\mathcal{N}} \chi_{[\theta,\theta+\Delta\theta]}(\theta^{(i)}) \chi_{[\varphi,\varphi+\Delta\varphi]}(\varphi^{(i)}), \end{aligned} \tag{29}$$

where $(\theta^{(i)}, \varphi^{(i)})$ are the polar and the azimuth angle of $\boldsymbol{\xi}^{(i)}$ and $\chi_A(x)$ is the characteristic function: it takes unity when $x \in A$ and zero otherwise. The results of the above sample counting (29) are to be compared with the following intensity distribution $I_{\rm CL}$ for the CL model (5):

$$\begin{aligned} I_{\rm CL} = &\frac{1}{|\xi_{\rm in1}|} \int_0^\infty d\xi\, \frac{\xi^2 \xi_1}{2\pi (RT_w)^2} \frac{|\xi_{\rm in1}|}{\alpha_t(2-\alpha_t)\alpha_n} I_0\left(\frac{\xi_1 \xi_{\rm in1}}{RT_w} \frac{\sqrt{1-\alpha_n}}{\alpha_n}\right) \\ &\times \exp\left(-\frac{\xi_1^2 + \xi_{\rm in1}^2(1-\alpha_n)}{2RT_w\alpha_n}\right) \exp\left(-\frac{|\boldsymbol{\xi}_\parallel - \boldsymbol{\xi}_{\rm in\parallel}(1-\alpha_t)|^2}{2RT_w\alpha_t(2-\alpha_t)}\right) \end{aligned}$$

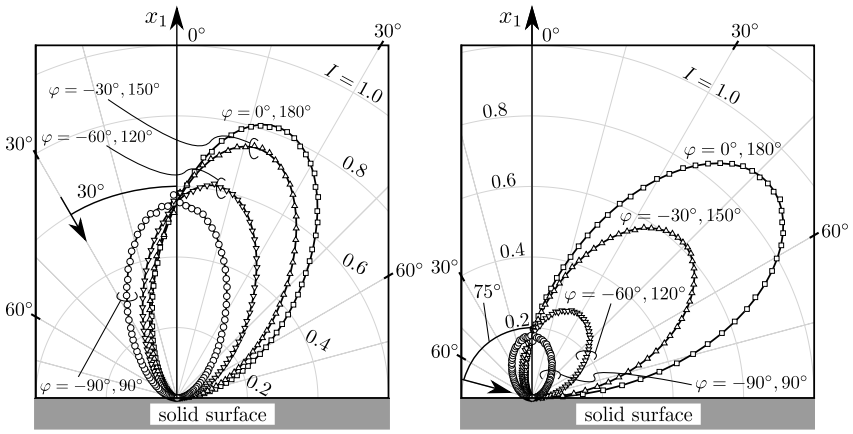

Fig. 3 In-plane and off-plane reflections of the mono-collimated molecular beam obtained by 10^8 particle simulations of the Langevin system (19): the case $\alpha_n = 0.3$ and $\alpha_t = 0.1$. The speed of the incident molecule is set as $|\boldsymbol{\xi}_{\rm in}|/\sqrt{2RT_w} = 0.522394$. (a) $\theta_{\rm in}^{\rm C} = 30°$, (b) $\theta_{\rm in}^{\rm C} = 75°$, where $\theta_{\rm in}^{\rm C} (\equiv \pi - \theta_{\rm in})$ is the angle of incidence of the velocity of the molecular beam $\boldsymbol{\xi}_{\rm in}$. φ is the azimuth angle measured clockwise from the direction of the projection of $\boldsymbol{\xi}_{\rm in}$ to the ξ_2-ξ_3 plane ($-\pi < \varphi \le \pi$). Symbols indicate the simulation results. Corresponding $I_{\rm CL}$'s in (30) are also shown for reference by solid lines. The arrow in each panel indicates the direction of $\boldsymbol{\xi}_{\rm in}$. Note the relation (31). The Milstein scheme with $\Delta t = 0.002\, d/\sqrt{2RT_w}$ and $p = 2$ has been used.

$$
\begin{aligned}
&= \frac{1}{2\pi (RT_w)^2} \frac{\cos\theta}{\alpha_t(2-\alpha_t)\alpha_n} \int_0^\infty d\xi\, \xi^3 I_0\Big(\frac{\xi \xi_{\rm in} \cos\theta \cos\theta_{\rm in}}{RT_w} \frac{\sqrt{1-\alpha_n}}{\alpha_n}\Big) \\
&\quad \times \exp\Big(-\frac{\xi^2 \sin^2\theta + \xi_{\rm in}^2 \sin^2\theta_{\rm in}(1-\alpha_t)^2}{2RT_w\alpha_t(2-\alpha_t)} - \frac{\xi^2\cos^2\theta + \xi_{\rm in}^2 \cos^2\theta_{\rm in}(1-\alpha_n)}{2RT_w\alpha_n} \\
&\qquad + \frac{\xi\xi_{\rm in}\sin\theta_{\rm in}\sin\theta\cos(\varphi-\varphi_{\rm in})(1-\alpha_t)}{RT_w\alpha_t(2-\alpha_t)}\Big).
\end{aligned} \tag{30}
$$

Figure 3 shows a couple of comparisons of the simulation results of (29) to (30). Good agreement is achieved, telling that the present construction of the Langevin system is appropriate. In the numerical simulations of the Langevin system, the Milstein scheme [10] has been adopted to achieve a sufficient numerical convergence with respect to the time-step size, see Sec. 5.3. Comparisons are made in the figure by using the relation between the parameters (α_n, α_t) and (ℓ_n, ℓ_t, d) in [4]:[3]

$$
\alpha_n = 1 - \exp\Big(-\frac{8d}{\ell_n}\Big), \quad \alpha_t = 1 - \exp\Big(-\frac{4d}{\ell_t}\Big). \tag{31}
$$

[3] There are misprints in (7.23) of [4], probably due to the inconsistent use of the notations ℓ_n and ℓ_t between [4] and [3].

5.3 Some aspects of the numerical method for the Langevin system

Probably the simplest and widespread numerical algorithm for solving the Langevin equation is the Euler–Maruyama method, the scheme of which reads in the present case

$$x_i^{(n+1)} = x_i^{(n)} + \xi_i^{(n)}\Delta t, \quad (i = 1,2,3), \tag{32a}$$

$$\xi_1^{(n+1)} = \xi_1^{(n)} - \frac{2}{\ell_n}\{|\xi_1^{(n)}|\xi_1^{(n)} - \frac{\xi_1^{(n)}}{|\xi_1^{(n)}|}RT_w\}\Delta t + 2\sqrt{RT_w\frac{|\xi_1^{(n)}|}{\ell_n}\Delta t}\Delta B_1^{(n)}, \tag{32b}$$

$$\xi_2^{(n+1)} = \xi_2^{(n)} - \frac{2}{\ell_t}|\xi_1^{(n)}|\xi_2^{(n)}\Delta t + 2\sqrt{RT_w\frac{|\xi_1^{(n)}|}{\ell_t}\Delta t}\Delta B_2^{(n)}, \tag{32c}$$

$$\xi_3^{(n+1)} = \xi_3^{(n)} - \frac{2}{\ell_t}|\xi_1^{(n)}|\xi_3^{(n)}\Delta t + 2\sqrt{RT_w\frac{|\xi_1^{(n)}|}{\ell_t}\Delta t}\Delta B_3^{(n)}. \tag{32d}$$

Here, $x_i^{(n)} = x_i(t_n)$, $\xi_i^{(n)} = \xi_i(t_n)$, $t_n = n\Delta t$ $(n = 0,1,2,\dots)$ is the discretised time, Δt is the size of time step, and $\Delta B_i^{(n)}$ $(i = 1,2,3)$ are mutually independent standard Gaussian random variables and are related to W_i as $\sqrt{\Delta t}\Delta B_i^{(n)} = W_i(t_{n+1}) - W_i(t_n)$. The Euler–Maruyama scheme is 1/2-order in the strong-order of convergence. In fortunate cases where S_{ij} is constant, the scheme becomes first-order [10, 9], which does not apply in the present case because of (18c). Indeed, the implementation of the Euler–Maruyama scheme shows a very slow convergence with respect to the size of time discretisation, see Fig. 4(a). The difficulty of the slow convergence is, however, resolved dramatically by switching to the Milstein scheme, which is known to be first-order in the strong-order of convergence [10], see Fig. 4(b). In the present case, as the noise is not commutative[4] for ξ_2 and ξ_3, the scheme becomes rather complicated as[5]

$$\begin{aligned}\xi_1^{(n+1)} = \xi_1^{(n)} &- \frac{2}{\ell_n}(|\xi_1^{(n)}|\xi_1^{(n)} - \frac{\xi_1^{(n)}}{|\xi_1^{(n)}|}RT_w)\Delta t + 2\sqrt{RT_w\frac{|\xi_1^{(n)}|}{\ell_n}\Delta t}\Delta B_1^{(n)} \\ &+ \frac{\xi_1^{(n)}}{|\xi_1^{(n)}|}\frac{2RT_w}{\ell_n}I_{11}^{(n)},\end{aligned} \tag{33a}$$

$$\xi_2^{(n+1)} = \xi_2^{(n)} - \frac{2}{\ell_t}|\xi_1^{(n)}|\xi_2^{(n)}\Delta t + 2\sqrt{RT_w\frac{|\xi_1^{(n)}|}{\ell_t}\Delta t}\Delta B_2^{(n)} + \frac{\xi_1^{(n)}}{|\xi_1^{(n)}|}\frac{2RT_w}{\sqrt{\ell_t\ell_n}}I_{12}^{(n)p}, \tag{33b}$$

[4] The noise is said to be commutative, if $\Theta_{\alpha i}$ in (13a) satisfies the condition $\Theta_{\beta i}(\partial\Theta_{\alpha j}/\partial y_\beta) = \Theta_{\beta j}(\partial\Theta_{\alpha i}/\partial y_\beta)$.

[5] See [10], pp. 346–347 for the details. Unfortunately, there are misprints in the corresponding formula in Sec. 6.4.3 of [9], though the latter reference is an excellent textbook. Incidentally, in [9], the Milstein scheme for the non-commutative noise is referred to as Kloeden and Platen's approximation.

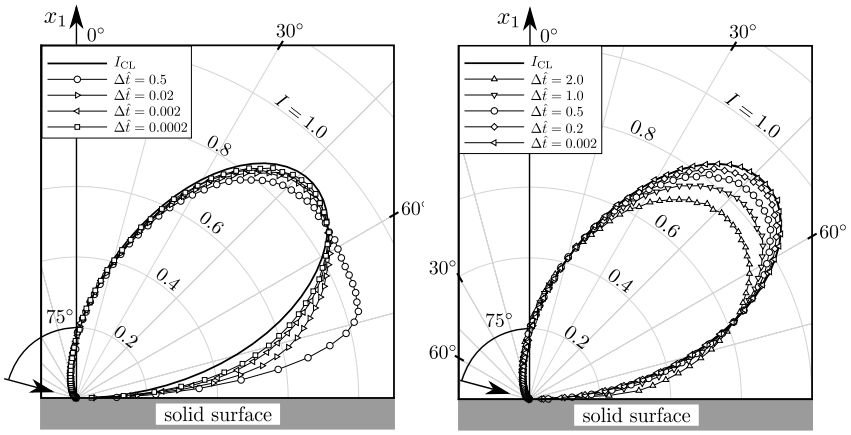

Fig. 4 Numerical convergence: the Euler–Maruyama scheme vs. the Milstein scheme. The results for the in-plane reflection of molecules ($\varphi = 0°,\ 180°$) for the same parameters as Fig. 3(b), except for the time step. (a) The Euler–Maruyama scheme, (b) the Milstein scheme with $p = 2$. Here, $\Delta\hat{t} = (\sqrt{2RT_w}/d)\Delta t$. Symbols indicate the simulation results, while thick solid lines indicate I_{CL} in (30). Note the difference of $\Delta\hat{t}$ between (a) and (b). Common symbols are used for common values of $\Delta\hat{t}$.

$$\xi_3^{(n+1)} = \xi_3^{(n)} - \frac{2}{\ell_t}|\xi_1^{(n)}|\xi_3^{(n)}\Delta t + 2\sqrt{RT_w\frac{|\xi_1^{(n)}|}{\ell_t}\Delta t}\Delta B_3^{(n)} + \frac{\xi_1^{(n)}}{|\xi_1^{(n)}|}\frac{2RT_w}{\sqrt{\ell_t\ell_n}}I_{13}^{(n)p}, \quad (33c)$$

where

$$I_{11}^{(n)} = \frac{\Delta t}{2}\{(\Delta B_1^{(n)})^2 - 1\}, \quad (34a)$$

$$I_{12}^{(n)p} = \frac{\Delta t}{2}\Delta B_1^{(n)}\Delta B_2^{(n)} + \frac{\Delta t}{2\pi}\sum_{q=1}^{p}\frac{1}{q}\{\zeta_{2q}(\sqrt{2}\Delta B_1^{(n)} - \eta_{1q}) - \zeta_{1q}(\sqrt{2}\Delta B_2^{(n)} - \eta_{2q})\} + \Delta t\sqrt{\rho^{(p)}}(\mu_2^{(p)}\Delta B_1^{(n)} - \mu_1^{(p)}\Delta B_2^{(n)}), \quad (34b)$$

$$I_{13}^{(n)p} = \frac{\Delta t}{2}\Delta B_1^{(n)}\Delta B_3^{(n)} + \frac{\Delta t}{2\pi}\sum_{q=1}^{p}\frac{1}{q}\{\zeta_{3q}(\sqrt{2}\Delta B_1^{(n)} - \eta_{1q}) - \zeta_{1q}(\sqrt{2}\Delta B_3^{(n)} - \eta_{3q})\} + \Delta t\sqrt{\rho^{(p)}}(\mu_3^{(p)}\Delta B_1^{(n)} - \mu_1^{(p)}\Delta B_3^{(n)}), \quad (34c)$$

$$\rho^{(p)} = \frac{1}{12} - \frac{1}{2\pi^2}\sum_{q=1}^{p}\frac{1}{q^2}. \quad (34d)$$

Here, $\mu_i^{(p)}$, η_{iq}, and ζ_{iq} are mutually independent standard Gaussian random vari-

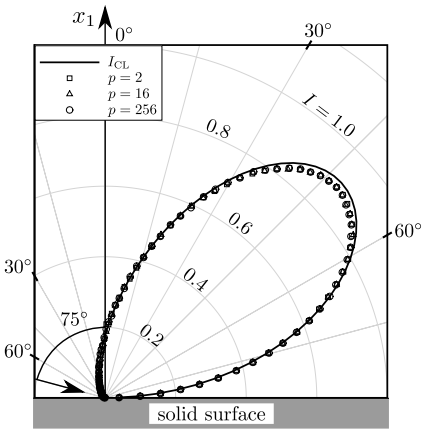

Fig. 5 Influence of the truncation number p in the Milstein scheme: the in-plane reflection of molecules ($\varphi = 0°$, $180°$) for the same parameters as Fig. 3(b), though a coarser time step $\Delta t = 0.2\, d/\sqrt{2RT_w}$ is used here. Symbols indicate the simulation results, while the solid line indicates I_{CL} in (30).

ables,[6] and p is the truncation number of the infinite series, which should be chosen so that $p > C/\Delta t$ for a positive constant C. As is clear from (33) and (34), the Milstein scheme requires the generation of $6(p + 1)$ standard Gaussian variables at each time step, which is $2(p + 1)$-times as many as in the Euler–Maruyama scheme and looks a serious drawback at a glance. Fortunately, however, numerical experiments show that the convergence rate with respect to p is excellent and that the setting $p = 2$ is found to be good enough, see Fig. 5.

5.4 A further observation: Some features of time delay in exit

We have so far focused on the way to construct the scattering kernel and/or the reflection intensity distribution without time delay. The scattering model without time delay supposes that the time duration of interaction with the wall is so short that the process may be regarded to occur instantaneously in the time scale of our interest. However, if we change the sample counting to that at a specified exit time τ, a closer observation of the dynamics is possible. It would also give a hint toward

[6] Originally, $\mu_i^{(p)}$ is defined as

$$\mu_i^{(p)} = \frac{1}{\sqrt{\rho^{(p)}\Delta t}} \sum_{q=p+1}^{\infty} \frac{1}{\pi q} \sqrt{\frac{\Delta t}{2}}\, \zeta_{iq}.$$

According to [10], however, $\mu_i^{(p)}$ thus defined becomes a standard Gaussian random variable. This property is very useful from the actual computational point of view.

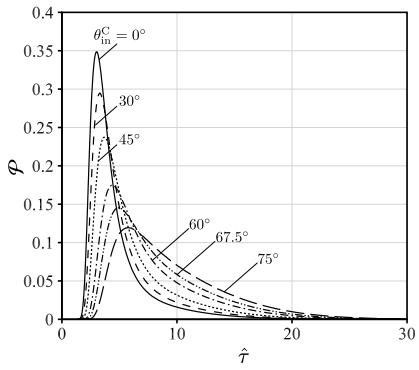

Fig. 6 Distribution of reflected molecules with respect to the exit time τ for various angle of incidence $\theta_{\rm in}^{\rm C}$. The parameters are the same as Fig. 3, except for a part of values of $\theta_{\rm in}^{\rm C}$. Here $\mathcal{P}(\hat{\tau}) = \sum_{i=1}^{\mathcal{N}} \chi_{[\hat{\tau},\hat{\tau}+\Delta\hat{\tau}]}/(\mathcal{N}\Delta\hat{\tau})$ with $\hat{\tau} = \tau(2RT_w)^{1/2}/d$, $\Delta\hat{\tau} = 0.05$, and $\mathcal{N} = 10^8$.

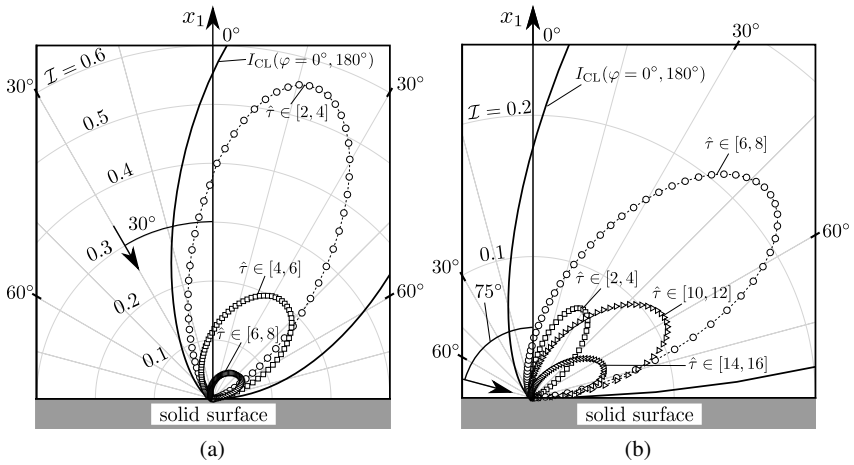

Fig. 7 Time-dependent in-plane reflection intensity distribution $\mathcal{I}$: the same case as Fig. 3. (a) $\theta_{\rm in}^{\rm C} = 30°$, (b) $\theta_{\rm in}^{\rm C} = 75°$. $\mathcal{I}$ is computed by the sample counting $\mathcal{I}(\hat{\tau} \in A, \theta, \varphi)\Delta\hat{\tau}_A \sin\theta\Delta\theta\Delta\varphi = (1/\mathcal{N})\sum_{i=1}^{\mathcal{N}} \chi_A(\hat{\tau}^{(i)})\chi_{[\theta,\theta+\Delta\theta]}(\theta^{(i)})\chi_{[\varphi,\varphi+\Delta\varphi]}(\varphi^{(i)})$, where $\mathcal{N} = 10^{10}$, $\Delta\hat{\tau}_A$ is the size of time interval A, and $\hat{\tau}^{(i)}$ is the dimensionless time of exit of the i-th sample. See the caption of Fig. 6.

the construction of the scattering kernel with a time-delay effect. Here, we present a few examples of such sample counting as well.

Figure 6 shows the distribution of the exit time of samples in the same simulation as Fig. 3. As is observed, the larger the angle of incidence is, the longer the time duration of interaction is. We have also observed that there are no test particles that experience the reversal of motion in the normal direction except for the reflection at the potential barrier [see also Fig. 2(c)]. Hence, they commonly travel $2d$ in depth.

These numerical observations suggest that in the CL model molecules of tangential incidence have more chance to remain at a low speed in the normal direction, and thus to need a longer time duration before leaving.

The common travelling distance $2d$ in depth implies that $\int |\xi_1| dt = 2d$ holds, so that the *drift*-part deceleration yields $\boldsymbol{\xi}_{\parallel} = \boldsymbol{\xi}_{\mathrm{in}\parallel} \exp(-4d/\ell_t) = \boldsymbol{\xi}_{\mathrm{in}\parallel}(1-\alpha_t)$ at the exit time; see (21). This coincides with the central velocity of the Gaussian in tangential directions in the kernel of CL model; see (5). Finally, an example of the in-plane reflection intensity distribution in a specified interval of exit time is shown in Fig. 7. The distribution inclines more to the tangential direction for the molecules of larger exit time.

6 Conclusion

In the present paper, we have revisited the Cercignani–Lampis model for the gas–surface interaction, along the lines of Cercignani in [4]. Starting from his time-independent Fokker–Planck system, we have introduced its simple and natural time-dependent extension and have identified the corresponding Langevin system.

In the Langevin system, there are two types of interactions with the wall. One is a stochastic thermal agitation, which we call the *diffusion* part, and the size of agitation depends on the random variable ξ_1. The other is what we call the *drift* part, which leads $|\xi_1|$ toward the speed of kinetic energy given by the equipartition law. In the tangential directions it decelerates the molecule by the viscous-like drag proportional to the moment transferred by that molecule.

The appropriate sample counting of the Langevin system simulation has also been discussed, and the capability of reproducing the scattering kernel and/or the reflection intensity distribution have been numerically demonstrated. It has also been remarked that the present stochastic noise causes the application of the Euler–Maruyama method to be inefficient and requires the Milstein method.

Finally, we stress that, from a numerical point of view, the Langevin system is advantageous to the FP system in that the incident mono-collimated molecular beam is easily handled to allow a close observation as in Sec. 5.4. Indeed, the sampling there gives a way toward a construction of the time-delay effect in the scattering model. Such an extension has a potential importance for such as an evacuation-speed prediction in vacuum technologies. Modifications of the dynamics by coupling with strong scatterings suggested in [4] will also be possible in the same numerical framework, if desired. Unlike the concise expression of the original CL model, the extensions above suggested might require a data fitting to construct a ready-to-use kinetic boundary condition. Nevertheless, a flexibility of the present simple approach is an advantage of modern computational facilities over the tools/techniques available in 70's.

Appendix

The numerical simulation of the Langevin system is performed particle by particle. The process of computations for each test particle, say k-th particle ($k = 1, 2, \dots$), is as follows.

Suppose that the size of time step Δt is given. Set the initial position $\boldsymbol{x}^{(0)}$ and velocity $\boldsymbol{\xi}^{(0)}$ of the test particle as $\boldsymbol{x}^{(0)} = \boldsymbol{0}$ and $\boldsymbol{\xi}^{(0)} = \boldsymbol{\xi}_{\mathrm{in}}$. Let $\boldsymbol{x}^{(n)}$ and $\boldsymbol{\xi}^{(n)}$ be known, where $x_1^{(n)} \in [-d, 0]$ and $n = 0, 1, 2, \dots$

Step 1. Compute the particle position $\boldsymbol{x}^{(n+1)}$ at time $t^{(n+1)}$ by (32a). If $x_1^{(n+1)} < -d$, discard it and reset $x_1^{(n+1)}$ as $x_1^{(n+1)} = -2d - x_1^{(n)} - \xi_1^{(n)}\Delta t$. This is due to the specular reflection at the potential barrier.

Step 2. Compute the particle velocity $\boldsymbol{\xi}^{(n+1)}$ at time $t^{(n+1)}$ by (33) with (34).

2a. If $x_1^{(n+1)} < -d$ occurs in Step 1, change the sign of $\xi_1^{(n+1)}$; then go to 2c.

2b. If $x_1^{(n+1)} > 0$, put $\Delta t^\sharp = \Delta t - x_1^{(n+1)}/\xi_1^{(n)}$, and compute $\boldsymbol{x}^\sharp$ and $\boldsymbol{\xi}^\sharp$ by (32a) and (33) using $\Delta t^\sharp$ in place of Δt. If $\xi_1^\sharp \geq 0$, which is the case usually, record $n\Delta t + \Delta t^\sharp$, $\boldsymbol{x}^\sharp$, and $\boldsymbol{\xi}^\sharp$ as the exit instance, position, and velocity of the k-th particle, and stop the computation. In case $\xi_1^\sharp < 0$ happens to occur, continue the computation to reset $\boldsymbol{x}^{(n+1)}$ and $\boldsymbol{\xi}^{(n+1)}$ by (32a) and (33) using $(\Delta t - \Delta t^\sharp)$, $\boldsymbol{x}^\sharp$, and $\boldsymbol{\xi}^\sharp$ in place of Δt, $\boldsymbol{x}^{(n)}$, and $\boldsymbol{\xi}^{(n)}$; then go to 2c.

2c. If $x_1^{(n+1)} \leq 0$, go back to Step 1 and shift n to $n + 1$.

Repeat the above steps until an enough number of samples have been collected. In the actual computations, the Mersenne Twister pseudo-random number generator [14] has been used in generating the standard Gaussian variables.

Acknowledgements The present work has been supported in part by JSPS KAKENHI Grant No. 17K18840 and by the Japan-France Integrated Action Program (SAKURA) Grant No. JPJSBP120193219.

References

1. Aoki, K., Charrier, P., Degond, P.: A hierarchy of models related to nanoflows and surface diffusion. Kinet. Relat. Models **4**, 53–85 (2011), doi: 10.3934/krm.2011.4.53
2. Brull, S., Charrier, P., Mieussens, L.: Nanoscale roughness effect on Maxwell-like boundary conditions for the Boltzmann equation. Phys. Fluids **28**, 082004 (2016), https://doi.org/10.1063/1.4960024
3. Cercignani, C.: Scattering kernels for gas–surface interactions. Transp. Theory Stat. Phys. **2**, 27–53 (1972).
4. Cercignani, C.: The Boltzmann Equation and Its Applications. Springer, New York (1988), Chap. III.
5. Cercignani, C., Lampis, M.: Kinetic models for gas–surface interactions. Transp. Theory Stat. Phys. **1**, 101–114 (1971), https://doi.org/10.1080/00411457108231440

6. Cowling, T. G.: On the Cercignani–Lampis formula for gas–surface interactions. J. Phys. D: Appl. Phys. **7**, 781–785 (1974).
7. Gardiner, C. W.: Handbook of Stochastic Methods for Physics, Chemistry and the Natural Sciences, 2nd ed. Springer, Berlin (1985), Sec. 4.3.
8. Jackson, E. A.: Equilibrium Statistical Mechanics. Dover edition, New York (2000), Sec. 4.6.
9. Jacob, K.: Stochastic Processes for Physicists, Understanding Noisy Systems. Cambridge University Press, Cambridge (2010), Secs. 3.6–3.8.
10. Kloeden, P. E., Platen, E.: Numerical Solution of Stochastic Differential Equations. Springer, Berlin (1992).
11. Kogan, M. N.: Rarefied Gas Dynamics. Plenum, New York (1969), Sec. 2.10.
12. Kuščer, I., Mozina, J., Krizamic, F.: The Knudsen model of thermal accomodation. In: Dini, D., et al. (eds.) Rarefied Gas Dynamics, Vol. I, pp. 97–108, Editrice Tecnico Scientifica, Pisa (1971).
13. Lord, R. G.: Some extensions to the Cercignani–Lampis gas–surface scattering kernel. Phys. Fluids A **3**, 706–710 (1991), https://doi.org/10.1063/1.858076
14. Matsumoto, M., Nishimura, T.: Mersenne twister: a 623-dimensionally equidistributed uniform pseudo-random number generator. ACM Trans. Model. Comput. Simul. **8**, 3–30 (1998), doi: 10.1145/272991.272995
15. Schaaf, S. A.: Mechanics of rarefied gases, In: Flügge, S. (ed.) Handbuch der Physik, band VIII/2, pp.591–624. Springer, Berlin (1963).
16. Sone, Y.: Molecular Gas Dynamics, Birkhäuser, Boston (2007); Supplement is available from http://hdl.handle.net/2433/66098.
17. Williams, M. M. R.: A phenomenological study of gas–surface interactions. J. Phys. D: Appl. Phys. **4**, 1315–1319 (1971).
18. Yamanishi, N., Matsumoto, Y., Shobatake, K.: Multistage gas–surface interaction model for the direct simulation Monte Carlo Method. Phys. Fluids **11**, 3540–3552 (1999), https://doi.org/10.1063/1.870211